Impact of High-Level Controller Actions on Local Active End-Nodes in a Distribution Grid

Shahinur Rahman, Emin Ucer, and Mithat Kisacikoglu
Dept. of Electrical and Computer Engineering, The University of Alabama, Tuscaloosa, AL
Emails: srahman6@crimson.ua.edu, eucer@crimson.ua.edu, and mkisacik@ua.edu

***Abstract*—Power utility grid is going through a challenging transformation. Growing number of power electronic active end-nodes are connected to the grid to enable large-scale integration of electric vehicles (EVs), energy storage systems (ESSs), and distributed energy resources (DERs), which increase the importance for high-level controllers to maintain physical limits of an electrical network. In addition, each connected end-node has its own controller embedded into it. These various controllers make the power grid operation complex and further challenging. We aim to understand the operation of these high-level controller actions and their impact on the distribution grid. Therefore, in this study, we analyze the local end-node voltage relationship with total feeder power consumption in the presence of four high-level voltage regulating devices. To serve this purpose, an IEEE 37-bus test system is modified with on-load tap changer (OLTC), voltage regulator (VR), shunt capacitor bank, and volt-var controlled PV smart inverter. We ran four different dynamic simulation cases: (i) without any high-level controller, (ii) with only OLTC and VR, (iii) with only shunt capacitor bank, and (iv) with only volt-var controller. Then, we investigated local active end-node voltage variation and how it is related to substation power consumption. This work will help to understand grid dynamics in estimating global information from local measurements to develop distributed controllers more effectively.**

I. Introduction

Power utility grid is undergoing a transformation with integration of distributed energy resources (DERs), electric vehicles (EVs), and energy storage systems (ESSs). Large-scale integration of these will introduce many new active end-nodes to the network. Millions of active end-nodes will compete with each other for the opportunity of supplying or consuming electric power. The high number of these controllable and dynamic end-nodes will threaten the performance of the power system operation, quality of the power supplied, and reliability of the entire system. The advent of compact, more powerful, and high switching frequency power electronics integrated into these active nodes will further complicate the problem. Distribution system operators (DSOs) are continuously working to maintain all the end-node voltages within their limits with the help of high-level voltage regulating controllers (i.e., on-load tap changers (OLTCs), voltage regulators (VRs), and shunt capacitor banks). OLTC and VR act as a variable ratio transformer connecting the distribution network (DN) to the transmission network (TN) or placed within the DN to increase/decrease voltage as required. Shunt capacitor banks connected through mechanical breakers to the DNs inject reactive power to the grid for voltage boosting and/or power factor correction. In addition, many local controllers, i.e., PV inverters and EV chargers, will exist inside the distribution grid and may inject and/or absorb reactive power for voltage regulation. All these control mechanism make the power grid structure very complex.

Unpredictable supply of DERs and increasing loads at active end-nodes make the supply-demand balance extremely challenging. Control schemes are reported in the literature to dispatch power properly, shape peak loads, and utilize the existing substation transformer capacity [1]–[4]. Some of these control algorithms are built on local measurements only. However, local controllers are not efficient to use the grid's full capacity as they lack any external/global information [5]. In a distributed control approach, active end-nodes can communicate with other nodes and/or with a central location to get global status [6]. The communication between end-nodes and substation should be much less than real-time to reduce overhead and related operational costs [7]. However, the distributed controller may estimate global information from local observations if the global data is sent once after a certain period of time (e.g., day, week, or month). With the advent of machine learning techniques, it is possible to extract global information from local measurements in a continuous way [8]. To get a better accuracy, we need to reveal the relationship between local and global variables for all operating conditions. Once this relationship is built up, end-nodes may be able to detect any grid congestion implicitly and utilize the grid capacity more accurately by only using their local measurements.

Learning the relationship between local observations and the global picture is not an easy task. There are various factors that impact this relationship. First, the substation voltage will have some variations [9] affecting the linear relation even though it is usually tightly regulated at the feeder level. Second, distribution grid topology can change due to various reasons including system reconfiguration and expansion [10]. Third, there are number of voltage regulation devices, such as LTC, VR, and capacitor banks operating at different points in the network. They are very effective in changing the active end-node voltage and thus affect the relationship. All these factors change the grid dynamics and therefore require an analysis to understand the complex grid well. In this paper, we will first investigate the individual impact of high-level controllers on local active end-nodes and its relation with total feeder demand. For this purpose, IEEE-37 bus test system will be modified with an OLTC, a VR, a shunt capacitor bank, and a volt-var controlled PV farm. The rest of the paper is organized as follows. Section II provides a description of the test system and the high-level controller modeling. Section III

This material is based upon work supported by the National Science Foundation under Award No 1755996.

shows simulation results and discussion. Section IV provides the concluding remarks and plan for future study.

II. Description of Test System

A. Distribution System Modeling

For our study, we modeled a modified IEEE-37 bus test system in MATLAB-Simulink as shown in Fig. 1. It represents a three-phase AC distribution grid that operates at a nominal voltage of 4.8 kV. A synchronous generator (swing type, 230 kV) is added at the beginning of the test system as a lumped generation and transmission section. A three-phase two-winding substation transformer connects the transmission-end with the distribution side and converts the transmission voltage of 230 kV to the distribution voltage level of 4.8 kV. Twenty-six residential neighborhoods are connected to the test system as described in [11]. In total, the feeder supplies power to 416 residential customers. To model household load profile, we have used real and reactive power consumption data of a typical house in Alabama. An eGauge smart meter [12] installed to the house records one second resolution of active and reactive power consumption data. The recorded data is sent to the cloud using local Wi-Fi connection. The data is publicly available at the University of Alabama institutional repository [13]. The procedure described in [11] is used to model power profile of 416 houses. One example of such a household load profile is shown in Fig. 2. The overall distribution grid operates slightly over 950 KVA at peak hours.

B. Modeling of High-level Controllers

The IEEE-37 bus test system is modified with three voltage regulating devices: OLTC, VR and a 75 (25+50) kVAR switched capacitor bank. A three-phase 300 kW PV farm is also added to the system with a volt-var controller. The detailed models of these devices are described in the following subsections.

1) OLTC Modeling: A three-phase OLTC is modeled with the substation transformer of the test bus system. It regulates voltage at bus 701. Three multi-winding transformer blocks are used to model three phases of OLTC. Each phase has a regulation winding connected at primary side. The regulation winding has nine taps in total (eight taps marked as 1 to 8 and a 0 tap) that allows $\pm 10\%$ voltage regulation. Each transformer block is equipped with a reversing switch that allows the regulation winding to be connected either in additive or subtractive polarity. Tap 0 provides nominal voltage (230/4.8 kV) ratio. Each tap change provides a voltage correction of ± 0.0125 pu ($\pm 10\% \div 8$). The voltage regulation is performed by varying the transformer primary and secondary voltage ratio, V_2/V_1 as follows:

$$\frac{V_2}{V_1} = \frac{1}{1 + N.\Delta U} \times \frac{V_{nom2}}{V_{nom1}} \tag{1}$$

where N denotes the tap position; ΔU is the amount of voltage change per tap; V_{nom1} and V_{nom2} are the primary and secondary side nominal voltage of the transformer, respectively. $1/(1 + N\Delta U)$ is also called voltage correction factor.

The tap change of OLTC is controlled by a compensator circuit. Positive-sequence voltage (V_{mes}) measured at the regulation point bus 701 is provided as an input of the control

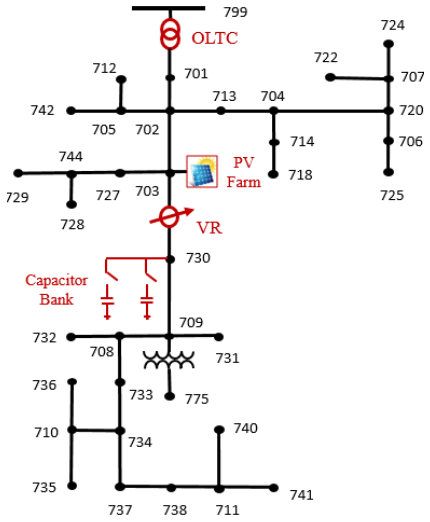

Figure 1: Modified IEEE-37 bus test system with OLTC, VR, shunt capacitor bank, and PV smart inverter.

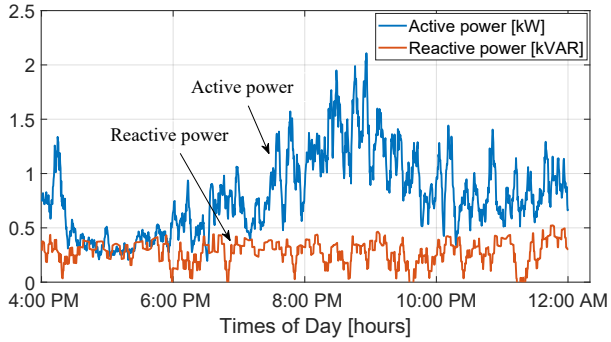

Figure 2: Sample active [kW] and reactive [kVAR] power consumption profile of a residential house.

circuit. Reference voltage (V_{ref}) is set to 1 pu. The OLTC will only change a tap if the condition in (2) sustains for a specific delay time, otherwise the tap will remain at the same position.

$$|V_{mes} - V_{ref}| > \text{dead band}/2 \tag{2}$$

where dead band is a user-defined variable for the allowable range of voltage variation at the regulation point. In this study, we have chosen 0.0375 pu as the dead band and 4 s as the delay time to observe OLTC tap changes within the existing loading environment.

2) Voltage Regulator Modeling: A VR is modeled by a three-phase transformer with a series tap changing mechanism as described in [14]. The VR is connected in series between bus 703 and 730. It also has eight taps and a reversing switch to provide $\pm 10\%$ regulation in both positive and negative polarity. The tap position is determined by a compensator circuit. An important task in modeling VR is to select a regulation node where voltage needs to be controlled and to measure the voltage of that node. In this study, the farthest node (741) of the test system is chosen as the regulation point since it faces the highest voltage drop. We measured the equivalent impedance (Z_{line}) and the current (I_{line}) flowing from the physical location of VR (bus 730) to the regulation node by a

steady-state analysis under maximum loading condition. The voltage (V_{mes}) at the regulation node is estimated by (3):

$$V_{mes} = V_{730} + I_{line} Z_{line} \tag{3}$$

where V_{730} denotes as the voltage of bus 730.

V_{mes} is provided as an input to the VR compensator circuit. The reference voltage (V_{ref}) is set to 1 pu. The taps of VR will only be changed if (2) holds true.

3) Switched Capacitor Bank Modeling: A 75 kVAR three-phase switched capacitor bank is modeled at bus 730 of the test system. It has two capacitor banks rated at 25 kVAR and 50 kVAR. The two capacitor banks inject reactive power to the grid and take part in voltage regulation. They are not connected to the grid all the time, rather they are switched on and off several times during a day. An automatic switch control is embedded on each capacitor bank, which senses a particular condition (i.e., node voltage). If the condition goes beyond their preset levels, the controller will initiate a trip signal to connect the capacitor bank to the power system. In this study, we have assumed two predefined trip signals to enable the switches of capacitor banks. When a switch is on, the corresponding capacitor will be connected to the grid.

4) PV Volt-Var Controller Modeling: A three-phase 300 kW PV farm is modeled by three controlled current sources and connected at bus 703. Active power generation data of a 50 kW PV farm is used and scaled up to 100 kW to model each phase of the PV farm. The active current (I_p) generated by the PV system is directly injected to the grid. I_p represents the current due to the active power (P_{PV}) portion of the PV system. As active PV current injection causes voltage rise to the bus 703, a volt-var controller is modeled to regulate the bus voltage as described in [15]. The controller takes the complex bus voltage, $\overline{V}_{703}$ as input and commands the required amount of reactive current (I_q) to be absorbed/injected to the inverter as output. I_q represents the current due to the reactive power (Q_{PV}) generation/absorption of the PV system. The total current, $\overline{I}_{PV}$ is the complex sum of I_p and I_q. The mathematical equations to find I_p, I_q, and I_{PV} are shown in (4):

$$\begin{aligned} I_p &= \frac{P_{PV}}{|\overline{V}_{703}|} \\ I_q &= \frac{Q_{PV}}{|\overline{V}_{703}|} \\ \overline{I}_{PV} &= I_p + jI_q \end{aligned} \tag{4}$$

A volt-var controller is characterized by three parameters: slope of the Volt-VAR (V-Q) controller characteristic curve, voltage set-point and lower and upper limits of VAR generation. We assumed a constant slope (X_s = 0.9) for V-Q characteristic curve and set the reference voltage to 1 pu. The PV inverter has S = 600 kVA rating. Then, the maximum reactive current, $\pm\ I_{q(max)}$ can be computed by $\sqrt{S^2 - P_{PV}^2}/|\overline{V}_{703}|$. As long as the injected/absorbed reactive current of PV stays within the maximum reactive current value ($\pm\ I_{q(max)}$), the voltage at bus 703 is regulated at the reference voltage.

III. Simulation Results and Analysis

To understand the actions of high-level controllers and their impacts on grid dynamics, we run four different simulation

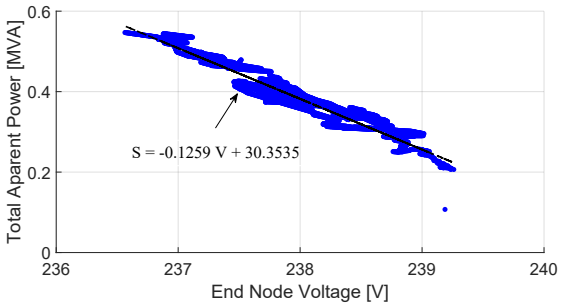

Figure 3: Total feeder power consumption vs. local active end-node voltage when all voltage regulation devices are disabled in the model.

cases: (i) without any high-level controller, (ii) with only OLTC and VR, (iii) with only capacitor bank, and (iv) with only PV inverter. In all simulations, the same household load profiles are used, and the model runs in the same time frame. We have chosen the simulation time from 4 PM to 12 AM to capture the grid peak loading and high voltage drops. First, the model runs with household loads only. Total substation power demand (S_{total}) and voltage at the farthest node (V_{end}) are recorded during the specified simulation time frame. To understand the relationship between S_{total} and V_{end}, an X/Y (scatter) plot is used with S_{total} along the vertical axis and V_{end} on the horizontal axis (Fig. 3). Each dot on the plot indicates V_{end} and the corresponding S_{total} at a sample time. The scatter plot with the simulation data is well fit with a straight line. The parameters of the linear line are estimated as $\theta_1 = -0.1259$ and $\theta_2 = 30.3535$. It is also observed that the voltage at the farthest node varies between $236\ -240\ V$, and the maximum consumed total feeder power is about $0.6\ MVA$.

Then, the model runs again with the same household loads keeping OLTC and VR enabled. The initial tap position of OLTC and VR are set to tap 0 positions. Figs. 4a and 4b show the time frame when OLTC/VR changes its tap and how the local active end-node voltage varies due to the tap change, accordingly. In the simulation time frame (4 PM-12 AM), OLTC does not change its tap since its regulation node is very close to the substation and faces less voltage drop severity. However, VR changes its tap three times (at 5:54 PM, 7:27 PM, and 7:41 PM). We have recorded S_{total} and the same V_{end} data and separated the data into four categories: part-A (4:00 PM-5:54 PM), part-B (5:55 PM-7:27 PM), part-C (7:28 PM-7:41 PM), and part-D (7:42 PM-12:00 AM). Part A and C denote the S_{total} and corresponding V_{end} data when VR was in tap position 0 and part B and D denote the S_{total} and corresponding V_{end} data when VR was in tap position 1. The data of all four categories are plotted in Fig. 5. It is found that S_{total} and V_{end} relationship is still linear in both tap positions 0 and 1 but the lines are shifted in parallel. Their relationship switches between two parallel lines when the tap of VR changes its position from 0 to 1 and vice versa. Both fitted lines in Fig. 5 have almost the same slope (-0.1411 vs. -0.1158) with a different intercept (33.9770 and 28.2960). We can conclude that the substation power and active end-node voltage relationship changes from a single line to a series of

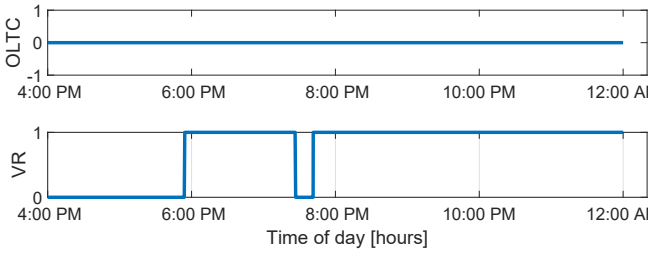

(a)

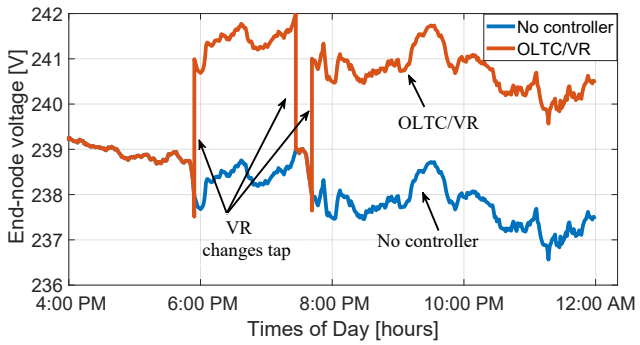

(b)

Figure 4: (a) Enable signals of OLTC and VR; and (b) voltage variation at the farthest active end-node due to the actions of OLTC and VR.

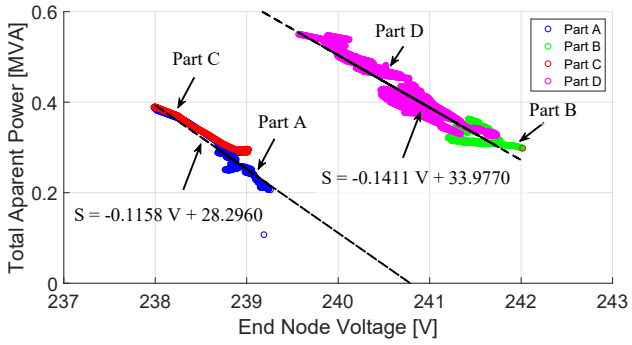

Figure 5: Total feeder power consumption vs. local active end-node voltage in the presence of OLTC and VR actions.

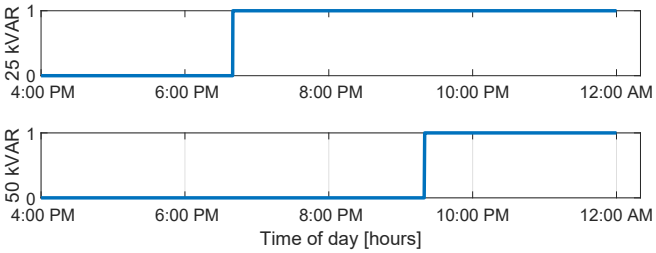

(a)

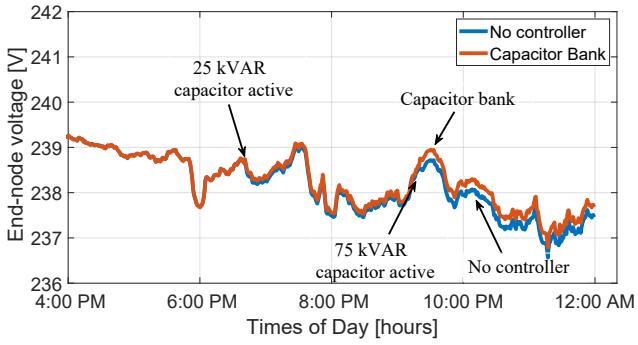

(b)

Figure 6: (a) Enable signals of 25 kVAR and 50 kVAR capacitor banks and (b) voltage variation at the farthest active end-node due to the actions of capacitor banks.

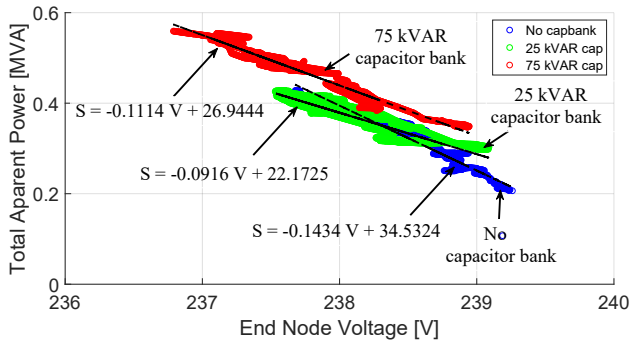

Figure 7: Total feeder power consumption vs. local active end-node voltage in the presence of capacitor banks actions.

parallel lines when the tap changes from one step to another. It is also observed that V_{end} varies between $238-242\ V$, slightly higher than the previous scenario. The operation of VR has shifted up the local active end-node voltage. The maximum total feeder power demand is seen to be the same as before due to the same household loading. The impact of OLTC on the S_{total} and V_{end} relationship is similar to VR since their operating principle is quite the same.

Next, we run the model with the same house loads and enable only the capacitor banks to operate. The switches connected to 25 kVAR and 50 kVAR capacitor are turned ON at 6:40 PM and 9:20 PM, respectively, and they remain ON for the rest of the simulation time. The capacitor bank switching signals are illustrated in Fig. 6a, and corresponding farthest active end-node voltage variations are shown in Fig. 6b. Fig. 6b shows that the local active end-node voltage increases when capacitors inject reactive power to the grid as expected. We have recorded S_{total} and the same V_{end} data and separated the data into three categories: no capacitor bank connected, 25 kVAR capacitor ON, and 75 (25+50) kVAR capacitor ON. The data of all categories are plotted in Fig. 7. Three separate lines in Fig. 7 illustrate the S_{total} and V_{end} relationship when no capacitor, 25 kVAR capacitor, and 75 kVAR capacitor connected to the grid. Fig. 7 shows that both the slope and intercept of S_{total} and V_{end} linear relationship changes due to the reactive power injection to the grid. We can conclude that the substation power and active end-node voltage relationship changes from a single line to a number of separate lines due to discrete amount of kVAR injection by the switched capacitor banks.

To understand the effects of continuous reactive power injection/absorption to the grid and its impact on S_{total} and V_{end} relationship, we have simulated the model with the same household loads and with a three-phase 300 kW volt-var controlled PV farm. The house loads are powered from the PV farm and the feeder itself. Injecting active power to the grid will cause a voltage rise to the node where it is connected at. Volt-var controller implemented in the PV inverter continuously injects/absorbs the required amount of reactive current to control that node voltage. Fig. 8a shows

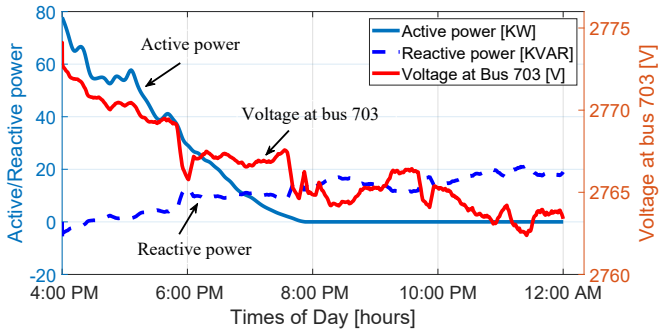

(a)

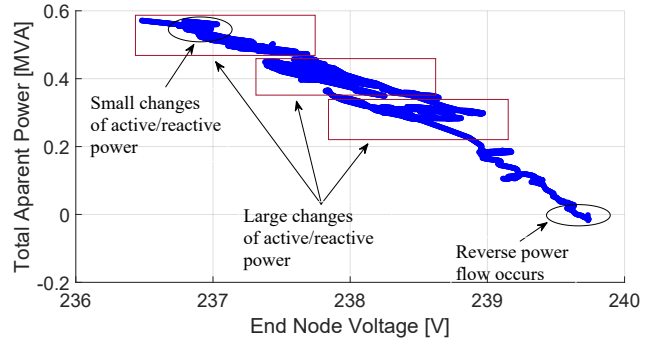

(b)

Figure 8: (a) Active and reactive power injected by the PV smart inverter and voltage variation at Bus 703, and (b) Total apparent power vs. local active end-node voltage relationship when PV volt-var controller was active only.

the active and reactive power injected by the PV farm and corresponding voltage change at bus-703. We have recorded S_{total} and the same V_{end} data and plotted the data in Fig. 8b. The S_{total} and V_{end} relationship changes its characteristic parameters continuously during the simulation time frame due to the change (small and/or large) of active and reactive power supplied/absorbed by the PV inverter. We have also noticed in Fig. 8b that V_{end} varies in between 236 -240 V. The maximum value of V_{end} is somewhat higher than the base case (model with house loads only). Injecting/absorbing reactive power to/from the smart PV inverter impacts the active end-node voltage, therefore, V_{end} have a closer value to the nominal voltage. At some point, the PV generates more power than the total load demand, which causes reverse power flow within the test system. The negative total apparent power in Fig. 8b represents the bi-directional power flow due to the excessive PV power generation.

IV. Conclusion

Power grid structure is complex and dynamic in nature. Large-scale integration of EVs, DERs and ESSs will make the system even more complex. Changing one component at one side of the system might have a big impact on the very far corner of the other side. It's hard to predict parameters and their relationship within this dynamic/changing environment. In this study, we have investigated the operation of high-level voltage regulating controllers; i.e., OLTC, VR, capacitor bank, and PV smart inverter and their impact on the relationship between total feeder apparent power and active end-node voltage. It is observed that the relation between substation power and end-node voltage is quite linear without any operation of high-level controllers. However, enabling OLTC/VR in the model changes the linear relation from a single line to multiple parallel lines. Discrete amount of reactive power injection to the grid creates several separate lines, whereas continuous injection/absorption of kVAR changes the characteristic parameters of the linear relationship. The understanding of high-level controller actions and their impact on local active nodes will help to estimate substation power from local measurements only. Therefore, the distributed controllers will able to detect congestion issues and utilize grid's full capacity. The future study will focus on developing the described cases in a real-time simulation environment.

References

[1] Y. Li, Z. Xu, and K. Meng, "Optimal power sharing control of wind turbines," *IEEE Trans. Power Syst.*, vol. 32, no. 1, pp. 824–825, Jan. 2017.

[2] N. G. Paterakis, O. Erdinc, A. G. Bakirtzis, and J. P. S. Catalao, "Optimal household appliances scheduling under day-ahead pricing and load-shaping demand response strategies," *IEEE Trans. Ind. Informat.*, vol. 11, no. 6, pp. 1509–1519, Dec. 2015.

[3] A. Ghazanfari, M. Hamzeh, and Y. A. I. Mohamed, "A resilient plug-and-play decentralized control for dc parking lots," *IEEE Trans. Smart Grid*, vol. 9, no. 3, pp. 1930 – 1942, Jan. 2018.

[4] J. Hu, C. Si, M. Lind, and R. Yu, "Preventing distribution grid congestion by integrating indirect control in a hierarchical electric vehicles' management system," *IEEE Trans. Transport. Electrific.*, vol. 2, no. 3, pp. 290–299, Sep. 2016.

[5] P. Richardson, D. Flynn, and A. Keane, "Local versus centralized charging strategies for electric vehicles in low voltage distribution systems," *IEEE Trans. Smart Grid*, vol. 3, no. 2, pp. 1020 – 1028, Jun. 2012.

[6] M. Chamana, B. H. Chowdhury, and F. Jahanbakhsh, "Distributed control of voltage regulating devices in the presence of high PV penetration to mitigate ramp-rate issues," *IEEE Trans. Smart Grid*, vol. 9, no. 2, pp. 1086 – 1095, Mar. 2018.

[7] Y. Jia, Z. Y. Dong, C. Sun, and K. Meng, "Cooperation-based distributed economic MPC for economic load dispatch and load frequency control of interconnected power systems," *IEEE Trans. Power Syst.*, vol. 34, no. 5, pp. 3964 – 3966, May 2019.

[8] E. Ucer, M. Kisacikoglu, A. Gurbuz, S. Rahman, and M. Yuksel, "A machine learning approach for understanding power distribution system congestion," in *IEEE Energy Conversion Congr. Expo. (ECCE)*, Oct. 2020, pp. 1–7.

[9] R. Huang, R. Fan, J. Daily, A. Fisher, and J. Fuller, "Open-source framework for power system transmission and distribution dynamics co-simulation," *IET Gener. Transm. Distrib.*, vol. 11, no. 12, pp. 3152 – 3162, Sep. 2017.

[10] J. Wen, Y. Tan, L. Jiang, and K. Lei, "Dynamic reconfiguration of distribution networks considering the real-time topology variation," *IET Gener. Transm. Distrib.*, vol. 12, no. 7, pp. 1509 – 1517, Mar. 2018.

[11] E. Ucer, M. C. Kisacikoglu, M. Yuksel, and A. C. Gurbuz, "An internet-inspired proportional fair EV charging control method," *IEEE Syst. J.*, vol. 13, no. 4, pp. 4292–4302, Dec. 2019.

[12] Energy monitoring systems for residential and commercial applications. http://www.egauge.net/. [Online; accessed 31-Jan-2018].

[13] E. Ucer, S. Rahman, A. McDonald, and M. Kisacikoglu. (2019) Residential active/reactive power consumption, voltage, and frequency data for a house in Alabama. [Dataset] https://ir.ua.edu/handle/123456789/6346. [Online; accessed 15-Jul-2020].

[14] W. H. Kersting, "Distribution feeder voltage regulation control," in *IEEE Rural Elect. Power Conf. (REPC)*, May 2009.

[15] A. Agrawal, K. Rahimi, R. P. Broadwater, and J. Bank, "Performance of PV generation feedback controllers: power factor versus volt-var control strategies," *IEEE North American Power Symposium*, Oct. 2015.